Mesocyclone-Targeted Doppler Velocity Dealiasing

QIN XU

NOAA/OAR/National Severe Storms Laboratory, Norman, Oklahoma

KANG NAI

Cooperative Institute for Mesoscale Meteorological Studies, University of Oklahoma, and
NOAA/OAR/National Severe Storms Laboratory, Norman, Oklahoma

ABSTRACT

The alias-robust variational (AR-Var) analysis developed originally for dealiasing raw velocities scanned from winter ice storms by operational WSR-88D radars was recently extended for dealiasing raw velocities scanned from all storms to increase the dealiased data coverage. The extended AR-Var (eAR-Var)-based dealiasing can detect tornadic mesocyclones and estimate their vortex center locations as by-products, but its dealiased data often leave rejected data holes in the critical vortex core and vicinity areas of detected mesocyclones. To solve this problem, a mesocyclone-targeted dealiasing routine is developed in this paper to perform two additional steps after the eAR-Var dealiasing. In particular, a reference check is performed in the first step, with the required reference velocities produced by a newly designed alias-robust vortex wind analysis to recover the rejected data in the vortex core, and then a continuity check is performed in the second step to recover the remaining rejected data around and beyond the vortex core. The mesocyclone-targeted dealiasing is tested extensively with severely aliased velocity data scanned from tornadic storms and is found to be effective and efficient for recovering the rejected data in and around the vortex core of the detected mesocyclone, provided the required data coverage conditions and analysis acceptance conditions are satisfied.

1. Introduction

Radar data quality control is indispensable and critical for radar data assimilation, and dealiasing is a very important and often very difficult part of radar velocity data quality control. The operationally used Doppler velocity dealiasing techniques (Eilts and Smith 1990; Jing and Wiener 1993; Witt et al. 2009) for processing WSR-88D radar data were developed primarily for visual applications and certain simple quantitative applications, such as automated mesocyclone detections (Stumpf et al. 1998; Smith and Elmore 2004). As these dealiasing techniques tend to retain as much as possible the original data coverage with considerable tolerance for bad or poor quality data, their processed data frequently contain errors (Burgess and Crum 2009; Witt et al. 2009) and thus often do not satisfy the high-quality standard required by data assimilation. To satisfy the need of radar data assimilation, efforts have been made

at NSSL in collaboration with other research institutes to develop robust dealiasing techniques (Gong et al. 2003; Gao et al. 2004; Zhang and Wang 2006; Xu et al. 2011; Xu and Nai 2012). As these dealiasing techniques were developed for data assimilation applications at the National Centers for Environmental Prediction (Liu et al. 2009), various stringent threshold conditions must be used to ensure the dealiased data to be completely free of error. These stringent conditions, however, tend to discard many data that cannot pass the thresholds, so the dealiased data often have less or even much less coverage than the raw data, especially in isolated data areas far away from the radar or in localized areas of strong and complex winds, such as those around mesocyclones.

To increase the dealiased data coverage but remain completely free of error, the alias-robust variational (AR-Var) analysis (Xu and Nai 2013) developed originally for dealiasing raw velocities scanned from winter ice storms by operational WSR-88D radars was extended adaptively and used in place of the alias-robust

---

velocity–azimuth display (AR-VAD) analysis (Xu et al. 2010) to produce more reliable reference velocities for dealiasing raw velocities scanned from all storms (Xu et al. 2013, hereinafter X13). In particular, model-predicted wind fields (such as those predicted by the NCEP operational Rapid Refresh model used in this paper) are interpolated onto selected range circles to obtain first-guess radial-component velocities for the adaptively extended AR-Var analysis to cover isolated data areas far away from the radar, so more raw data can pass the stringent threshold conditions used by the reference check in the first step. Also, new procedures were designed and added to the continuity check in the second (also last) step to further increase the dealiased data coverage, especially over areas threatened by severe storms and their generated tornadic mesocyclones. Such an extended AR-Var (eAR-Var)-based dealiasing, originally named model+AR-Var-based dealiasing in X13 but called eAR-Var dealiasing for short hereinafter in this paper, can also detect tornadic mesocyclones and estimate their vortex center locations as by-products. Its dealiased data, however, still often do not cover all the data points and thus leave rejected data holes in the critical vortex core and vicinity areas of a detected mesocyclone (see Figs. 2b, 3b, and 4b). To solve this problem, a mesocyclone-targeted dealiasing is developed to perform two additional steps after the eAR-Var dealiasing. The first step performs a reference check with the required reference velocities produced by a newly designed alias-robust (AR) vortex wind analysis to recover the rejected data in the vortex core, and the second step performs a continuity check to recover the remaining rejected data around and beyond the vortex core. The new AR vortex wind analysis uses the same vortex model as that used for tropical cyclones in Xu et al. (2014, hereinafter X14), but it retains all six control parameters to properly model mesocyclone winds on each tilt of the radar scan where a mesocyclone is detected and uses two-dimensional data over the vortex core area of the detected mesocyclone to estimate the six control parameters.

The parametric vortex model and cost function are presented in the next section. The required conditions on data coverage for performing the AR vortex wind analysis and the conditions for accepting the performed vortex wind analysis are detailed in section 3. The reference check used in the first step and the continuity check used in the second step of the mesocyclone-targeted dealiasing are described in section 4. Section 5 shows the test results with aliased velocities scanned by operational WSR-88D radars from tornadic mesocyclones. Conclusions follow in section 6.
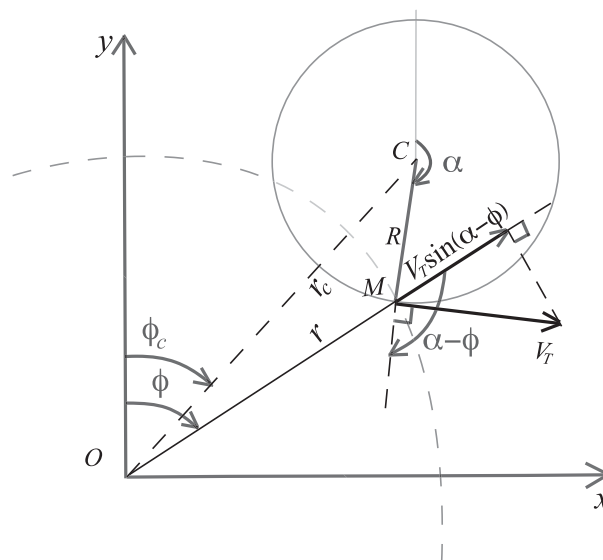

FIG. 1. Schematic diagram of vortex center location (marked by the letter C) and a circle of constant V_T with a radial distance of R from the vortex center in the coordinate system centered at the radar site (marked by the letter O). The dashed arc shows a part of the selected range circle (with a radial distance of r from the radar site), r_c is the distance from the radar site to the vortex center, and the letter M marks the measurement point on this selected circle. The tangential velocity of the modeled vortex at point M is shown by the arrow marked by V_T, and the radial component of this tangential velocity projected onto the radar beam direction is shown by the arrow marked by $V_T \sin(\alpha - \phi)$.

2. Vortex model and cost function

a. Parametric vortex model and modeled radial-component velocity

For the reference check in the first step of the mesocyclone-targeted dealiasing, the required reference velocity is produced by an AR vortex wind analysis designed specifically for mesocyclones. This AR vortex wind analysis uses the same vortex model of Vatistas et al. (1991) as that used for tropical cyclones in X14 but applies it to mesocylones instead of tropical cyclones. In this vortex model, the tangential velocity of the vortex V_T is merely a function of the radial distance from the vortex center R, and this function is formulated by

$$V_T = \sqrt{2} V_M (R/R_M)[1 + (R/R_M)^4]^{-1/2}, \tag{1}$$

where V_M is the maximum tangential velocity of the modeled vortex, and R_M is the radius of V_M (i.e., the distance C − M if $V_T = V_M$ at point M in Fig. 1). As shown in Fig. 2 and (5) of Vatistas et al. (1991), this vortex model is physically representative of many observed vortex profiles in fluid dynamics.

When the environmental mean wind (or mesocyclone translational velocity) is considered, the ground-relative horizontal wind vector (u, v) in and around a mesocyclone is modeled by

$$(u,v) = (V_e \sin\beta - V_T \cos\alpha, V_e \cos\beta + V_T \sin\alpha), \qquad (2)$$

where V_e and β denote the environmental horizontal wind speed and direction angle (with respect to the northward y coordinate), respectively; V_T is the tangential velocity modeled in (1) for a cyclonically rotating vortex; and α denotes the azimuthal angle viewed from the vortex center (as shown for point M in Fig. 1). Projecting (2) onto the radar beam direction gives the modeled radial-component velocity in the following form:

$$\begin{aligned} v_r^{\mathrm{md}} &\equiv (u\sin\phi + v\cos\phi)\cos\theta \\ &= [V_e \cos(\phi - \beta) + V_T \sin(\alpha - \phi)]\cos\theta, \qquad (3) \end{aligned}$$

where ϕ denotes the azimuthal angle viewed from the radar site (as shown for point M in Fig. 1), and θ is the tilt angle of the radar beam at the measurement point relative to Earth's surface below that measurement point.

As shown in (4b) and (4c) of X14, R and α are functions of (r, ϕ, r_c, ϕ_c) given implicitly by

$$R^2 = r^2 + r_c^2 - 2rr_c \cos(\phi - \phi_c) \qquad (4a)$$

and

$$\sin(\alpha - \phi) = (r_c/R)\sin(\phi - \phi_c). \qquad (4b)$$

Here, (4a) is the cosine formula applied to the CM side and (4b) is the sine formula applied to the OC and CM sides of the triangle COM in Fig. 1, r is the radial distance of the measurement point (M in Fig. 1) from the radar site, r_c is the distance from the radar site to the vortex center, and ϕ_c is the azimuthal angle of the vortex center viewed from the radar in the radar local coordinate system. Substituting (1) for V_T and (4) for R and α as functions of (r, ϕ, r_c, ϕ_c) into (3) gives v_r^{md} as a function of the location of the measurement point in the radar coordinates (r, ϕ, θ) and the six control parameters, denoted by $\mathbf{c} \equiv (V_M, R_M, r_c, \phi_c, V_e, \beta)$, of the modeled vortex plus environmental wind.

b. Cost function for AR vortex wind analysis

The newly designed AR vortex wind analysis retains all the abovementioned six control parameters in the modeled radial-component velocity v_r^{md} and its constructed cost function for analyzing mesocyclone winds. This is different from the vortex wind analysis in X14, which retains only two control parameters (V_M, R_M) in

the cost function for analyzing tropical cyclone winds. The modeled v_r^{md} in (3) is used to fit, in terms of least squares, all the available velocity data in an $L_x \times L_y$ square area, called the data-fitting area, which is co-centered with the mesocyclone on each tilt of radar scan where a mesocyclone is detected. Here, L_x (or L_y) is the side length of the data-fitting area in the x (or y) direction and is set empirically to 2 km for $r_c \leq 150$ km, to 3 km for $r_c > 150$ km at and below the 1.6° tilt, and to 6 km for $r_c > 150$ km above the 1.6° tilt. The vortex center location is estimated as a by-product by the eAR-Var dealiasing (X13). The least squares fit minimizes the following cost function:

$$J(\mathbf{c}) = \sum_i \{Z[v_r^{\mathrm{md}}(\mathbf{p}_i \,|\, \mathbf{c}) - v_r^{\mathrm{ob}}(\mathbf{p}_i), v_N]\}^2/m, \qquad (5)$$

where the summation is over i from 1 to m for all observations in the data-fitting area, $Z[(), v_N] \equiv () - 2v_N \mathrm{Int}[()/(2v_N)]$ is the aliasing operator, v_N is the Nyquist velocity, $\mathrm{Int}[()]$ represents the nearest integer of (), $\mathbf{p}_i \equiv (r_i, \phi_i, \theta_i)$ is the position vector to denote the ith measurement point in the radar coordinates, $v_r^{\mathrm{md}}(\mathbf{p}_i \,|\, \mathbf{c})$ denotes v_r^{md} modeled in (3) at the ith measurement point as a function of $\mathbf{c} \equiv (V_M, R_M, r_c, \phi_c, V_e, \beta)$, and $v_r^{\mathrm{ob}}(\mathbf{p}_i)$ denotes the raw velocity observation at the ith measurement point.

3. Data coverage conditions and analysis acceptance conditions

a. Required conditions on data coverage

To ensure the quality of the AR vortex wind analysis, the raw data coverage and the coverage of the processed and accepted data by the eAR-Var dealiasing, called seed data, are required to satisfy the following conditions:

1) The raw data cover no less than one-third of the data-fitting area (defined in section 2b).
2) The seed data cover no less than one-fourth of the data-fitting area and should be distributed on both sides (rather than only one side) of the radial that passes the estimated vortex center.
3) There are at least three rejected data in the data-fitting area.

The first condition is required because the vortex wind analysis needs to be performed reliably with sufficient amounts of raw data in and around the vortex core. The second condition is required because the seed data should have adequate coverage in the vortex core area. Otherwise, the vortex center location may not be reliably estimated by the eAR-Var dealiasing from its

produced seed data. The third condition is imposed for computational efficiency. If there are no more than two rejected data in the data-fitting area, then it is unnecessary to perform the AR vortex wind analysis because the gain is insignificant and unjustifiable by the computational cost.

b. Conditions for accepting the vortex wind analysis

The cost function in (5) is formulated with the aliasing operator based on the approach (Xu et al. 2009; Xu 2009) that can ensure the cost function to be smooth and concave upward in the vicinity of the global minimum. Thus, the global minimum can be found by using a descent algorithm if the initial guess of $(V_M, R_M, r_c, \phi_c, V_e, \beta)$ is adequately accurate in the vicinity of the global minimum. An adequately accurate initial guess of (V_e, β) can be obtained from the wind field produced by a numerical weather prediction system, and the wind field predicted by the NCEP operational Rapid Refresh model is used for this in this paper. As byproducts, (r_c, ϕ_c) and (V_M, R_M) can be estimated from the eAR-Var dealiasing (see the appendix of X13), but only the estimated (r_c, ϕ_c) can be adequately accurate and thus used as the initial guess. The estimated (V_M, R_M) are very sensitive to data holes (rejected by the eAR-Var dealiasing) in the vortex area and thus are often not accurate. As a remedy, multiple initial guesses of (V_M, R_M) are selected empirically with $V_M/v_N = 1, 1.7, 2.4, 3.1$, and 3.8 and $R_M = 0.1, 0.3, 0.5, 0.7$, and 0.9 km. This gives 5×5 sets of initial guesses with 25 different combinations of V_M and R_M, but one group of selected values of $(r_c, \phi_c, V_e, \beta)$ as described above. Each set is used to initialize the conjugate-gradient descent algorithm to search the minimum of J. The global minimum is given by the smallest among those from the 5×5 searched minima that satisfy the following conditions:

1) The fitting residual does not exceed $8.55 \, \text{m}^2 \, \text{s}^{-2}$; that is, min $J(\mathbf{c}) < 8.55 \, \text{m}^2 \, \text{s}^{-2}$.
2) The estimated V_M is between v_N and $70 \, \text{m} \, \text{s}^{-1}$.
3) The estimated R_M is between 0.2 and 2 km.
4) The estimated absolute values of $u_e = V_e \sin\beta$ and $v_e = V_e \cos\beta$ do not exceed 25 (40) m s^{-1} for $r_c < 150 \, \text{km}$ ($r_c \geq 150 \, \text{km}$).
5) In addition, the final estimated vortex center location (V_e, β) at the global minimum point must be still in the data-fitting area.

The abovementioned first condition requires the fitting to be sufficiently tight to filter out unreliable or poorly matched fittings. The next three conditions are imposed empirically based on the datasets so far tested to filter out possibly unrepresentative parameter values. The last condition is necessary to filter out severely dislocated fittings. As the abovementioned five conditions, called analysis acceptance conditions, need to be sufficiently stringent to filter out as cleanly as possible all unreliable or unrepresentative estimates, they may occasionally become overly stringent and thus reject truly representative estimates for some cases.

4. Refinement checks for mesocyclone-targeted dealiasing

a. Reference check in first step

The values of $(V_M, R_M, r_c, \phi_c, V_e, \beta)$ estimated by the AR vortex wind analysis at the global minimum point are substituted back into (1) to obtain the reference velocity at each rejected data point in the vortex core. Here, the vortex core is defined as the circular area within $R \leq R_c$ around the estimated vortex center at (r_c, ϕ_c), and R_c is the radial distance, where the modeled tangential velocity V_T equals the Nyquist velocity v_N outside R_M—the radius of V_M. By setting $V_T = v_N$ for $R = R_c$ in (1), R_c is solved as the positive root $(>R_M)$ in the following form:

$$R_c = R_M[V_M^2/v_N^2 + (V_M^4/v_N^4 + 1)^{1/2}].$$

The reference check is performed by using the same threshold conditions as in (3)–(5) of Xu et al. (2011) but applied only to rejected data in the vortex core defined above.

b. Continuity check in second step

The continuity check is performed in the second step using the same procedure as described for steps (v) and (vi) in section 3 of X13, but the procedure applies only to the remaining rejected data (both inside and outside the vortex core) over the entire tilt. By using the new seed data processed and accepted by the abovementioned reference check together with those produced by the eAR-Var dealiasing, this additional continuity check can recover (if the threshold conditions used by the continuity check are satisfied) the remaining rejected data over the entire tilt. This completes the mesocyclone-targeted dealiasing on the tilt where the mesocyclone is detected.

5. Test results

a. Tests with 10 volumes of severely aliased velocity data and example results

The mesocyclone-targeted dealiasing is tested with 10 volumes of severely aliased velocity data collected

(from 1951 to 2030 UTC) by the operational KTLX radar (Oklahoma City, Oklahoma) from the tornadic mesocyclone that produced EF5 tornado that struck Moore, Oklahoma, on 20 May 2013. When the eAR-Var dealiasing is first applied to these 10 volumes, its dealiased data leave significant data holes in and around many detected vortex cores. In particular, 2617 velocity data are rejected in 46 vortex cores (detected on 46 tilts scanned at different times). From these 2617 rejected data, the mesocyclone-targeted dealiasing can recover 2234 data, that is, more than 84% of the total rejected data in the abovementioned 46 vortex cores. Among these 46 vortex cores, the rejected data are recovered completely (100%) in 11 vortex cores, and this is shown by the examples presented below.

The first example is shown in Fig. 2 for the mesocyclone detected by the eAR-Var dealiasing on the 0.5° tilt of the KTLX radar scan at 2008:42 UTC 20 May 2013. As shown in Fig. 2a, the raw velocities were severely aliased in two small areas (marked by the two white A's) in the vortex core area. These aliased velocities are partially corrected and partially rejected by the eAR-Var dealiasing, and the rejected data points are shown by the black pixels in Fig. 2b. The initial guess of (r_c, ϕ_c) is given as a by-product from the eAR-Var dealiasing. Figure 2c shows the available data in the data-fitting area, and these available data consist of dealiased data produced by and raw data rejected by the eAR-Var dealiasing. Figure 2d shows the reference velocities produced over the vortex core by the AR vortex wind analysis (with the global minimum point found at $V_M = 49.2 \, \mathrm{m \, s^{-1}}$, $R_M = 0.340 \, \mathrm{km}$, $r_c = 26.864 \, \mathrm{km}$, $\phi_c = 265.8°$, $V_e = 12.65 \, \mathrm{m \, s^{-1}}$, and $\beta = 39.22°$ in the control parameter space). By comparing Figs. 2c and 2d, one can see that the fitting is not adversely affected by the aliased raw data (marked by white × symbols in Fig. 2c) in the data-fitting area, and this indicates that the analysis is indeed alias robust due to the use of the aliasing operator in the cost function [see (5)]. As the vortex core is well covered by the reference velocities, the rejected data in the vortex core are mostly recovered by the reference check with only three rejected data left in the vortex core as shown in Fig. 2e. These three rejected data in the vortex core and other remaining rejected data outside the vortex core are then recovered by the continuity check in the second step as shown in Fig. 2f. By performing the abovementioned two steps, the mesocyclone-targeted dealiasing is able to recover and correct not only all the 17 rejected data in the vortex core but also additional 431 rejected data (not fully shown) outside the vortex core over the entire tilt.

The second example is shown in Fig. 3 for the mesocyclone detected on the 2.4° tilt of the KTLX radar scan at 2018:48 UTC 20 May 2013. As shown in Fig. 3a, the raw velocities were aliased not only in the vortex core area but also at many individual pixels scattered outside the vortex core. Figure 3b shows that the eAR-Var dealiasing can correct only a part of the aliased velocities but many good data are also rejected. Figure 3c shows the available data in the data-fitting area. Figure 3d shows the reference velocities produced by the AR vortex wind analysis (with the global minimum point found at $V_M = 44.0 \, \mathrm{m \, s^{-1}}$, $R_M = 0.398 \, \mathrm{km}$, $r_c = 21.653 \, \mathrm{km}$, $\phi_c = 266.4°$, $V_e = 11.06 \, \mathrm{m \, s^{-1}}$, and $\beta = 29.81°$). Again, by comparing Figs. 3c and 3d, one can see that the fitting is not adversely affected by the aliased raw data in the data-fitting area. As shown in Fig. 3e, the rejected data in the vortex core are mostly recovered by the reference check with merely one rejected datum left in the vortex core. This rejected datum and many other remaining rejected data outside the vortex core are then corrected by the continuity check in the second step as shown in Fig. 3f. Through the abovementioned two steps, the mesocyclone-targeted dealiasing can recover and correct not only all the 58 rejected data in the vortex core but also 1447 rejected data (not fully shown) outside the vortex core over the entire tilt.

The third example is shown in Fig. 4 for the mesocyclone detected on the 5.1° tilt of the KTLX radar scan at 2010:50 UTC 20 May 2013. This is a rare case in which the eAR-Var dealiasing is not absolutely free of error. As shown in Fig. 4a, the raw velocities were severely aliased not only in the vortex core but also over a larger area to the southeast of the vortex core. Figure 4b shows that the dealiased data produced by the eAR-Var dealiasing contain not only a large rejected data hole but also seven erroneous velocities (marked by the small white x's in Fig. 4b) in the vortex core. Figure 4c shows the available data in the data-fitting area. Figure 4d shows the reference velocities produced by the AR vortex wind analysis (with the global minimum point found at $V_M = 38.9 \, \mathrm{m \, s^{-1}}$, $R_M = 0.496 \, \mathrm{km}$, $r_c = 25.836 \, \mathrm{km}$, $\phi_c = 266.9°$, $V_e = 11.18 \, \mathrm{m \, s^{-1}}$, and $\beta = 31.84°$). From Figs. 4c and 4d, one can see again that the fitting is not adversely affected by the aliased raw data in the data-fitting area. Thus, the reference check can be extended and applied to all the data (i.e., not only the rejected data but also the seed data) in the vortex core. With this extension, the erroneous velocities in the seed data are all corrected and the rejected data are mostly recovered in the vortex core with only three rejected data left in the vortex core area as shown in Fig. 4e. These three rejected data in the vortex core are then recovered by the continuity check as shown in Fig. 4f, and 477 rejected data are also recovered outside the vortex core over the entire tilt (not shown). The eAR-Var dealiasing is not absolutely free of error in only two
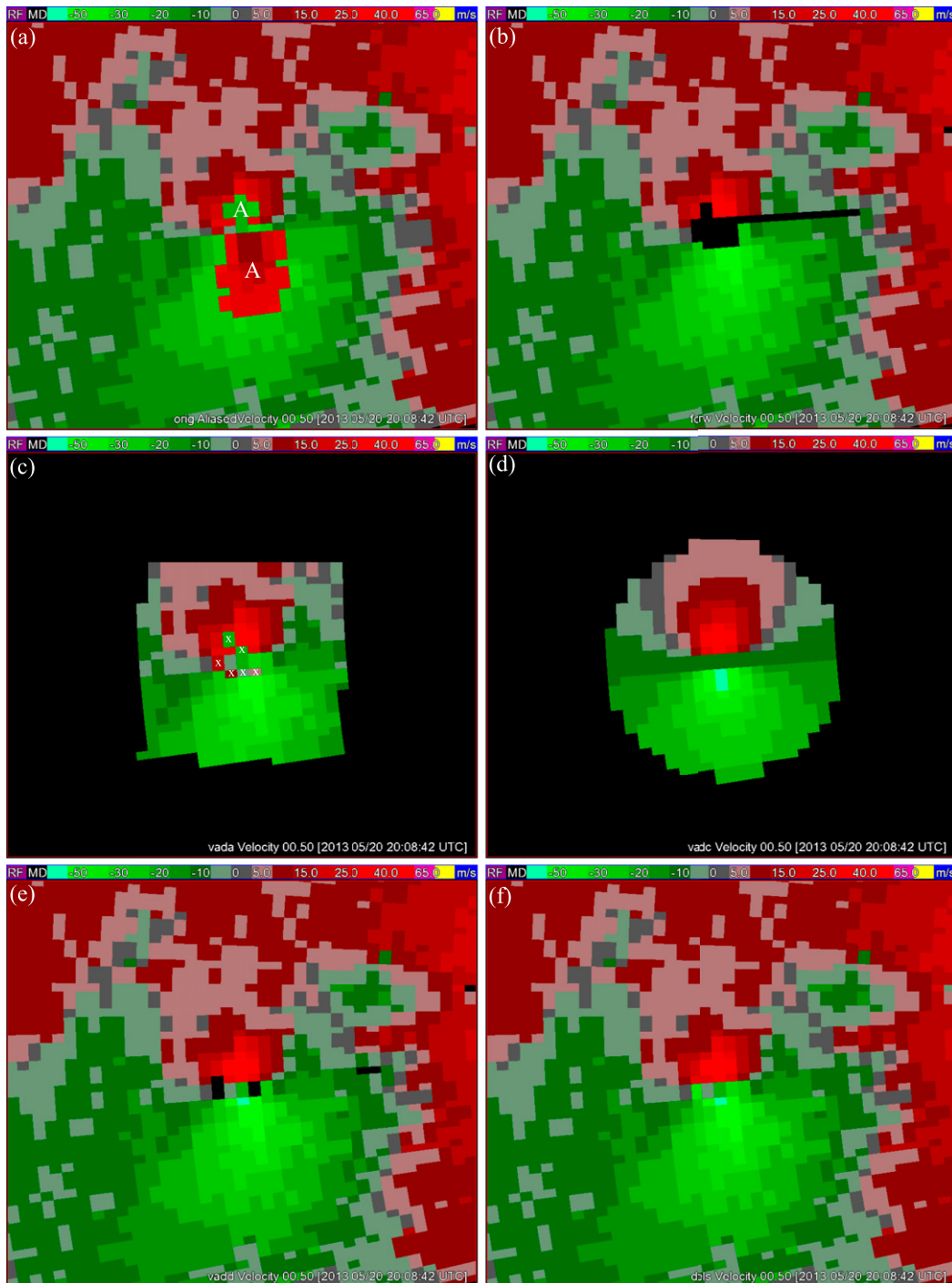
FIG. 2. (a) Image of raw velocity over and around the vortex core detected from the KTLX radar scan on the 0.5°
tilt (with Nyquist velocity $v_N = 26.12 \, \text{m s}^{-1}$, range gate resolution $\Delta r = 0.25 \, \text{km}$, and azimuth sampling interval
$\Delta\phi = 0.5°$) at 2008:42 UTC 20 May 2013 for the Moore tornadic mesocyclone. (b) Image of dealiased velocity
produced by the eAR-Var dealiasing (X13). (c) Image of available data (i.e., dealiased data plus raw data rejected
by the eAR-Var dealiasing) in the data-fitting area (defined in section 2b). (d) Image of reference velocity produced
over the vortex core by the AR vortex wind analysis. (e) Image of dealiased velocity produced by the reference
check in the first step. (f) Image of dealiased velocity produced by the continuity check in the second step of the
mesocyclone-targeted dealiasing. The two white A's in (a) mark the aliased velocity areas, respectively. The black
pixels in (b) show the rejected data by the eAR-Var dealiasing of X13. The six white x's in (c) mark the aliased raw
data, respectively. The color scale on the top of each panel shows red (green) for positive (negative) value, that is,
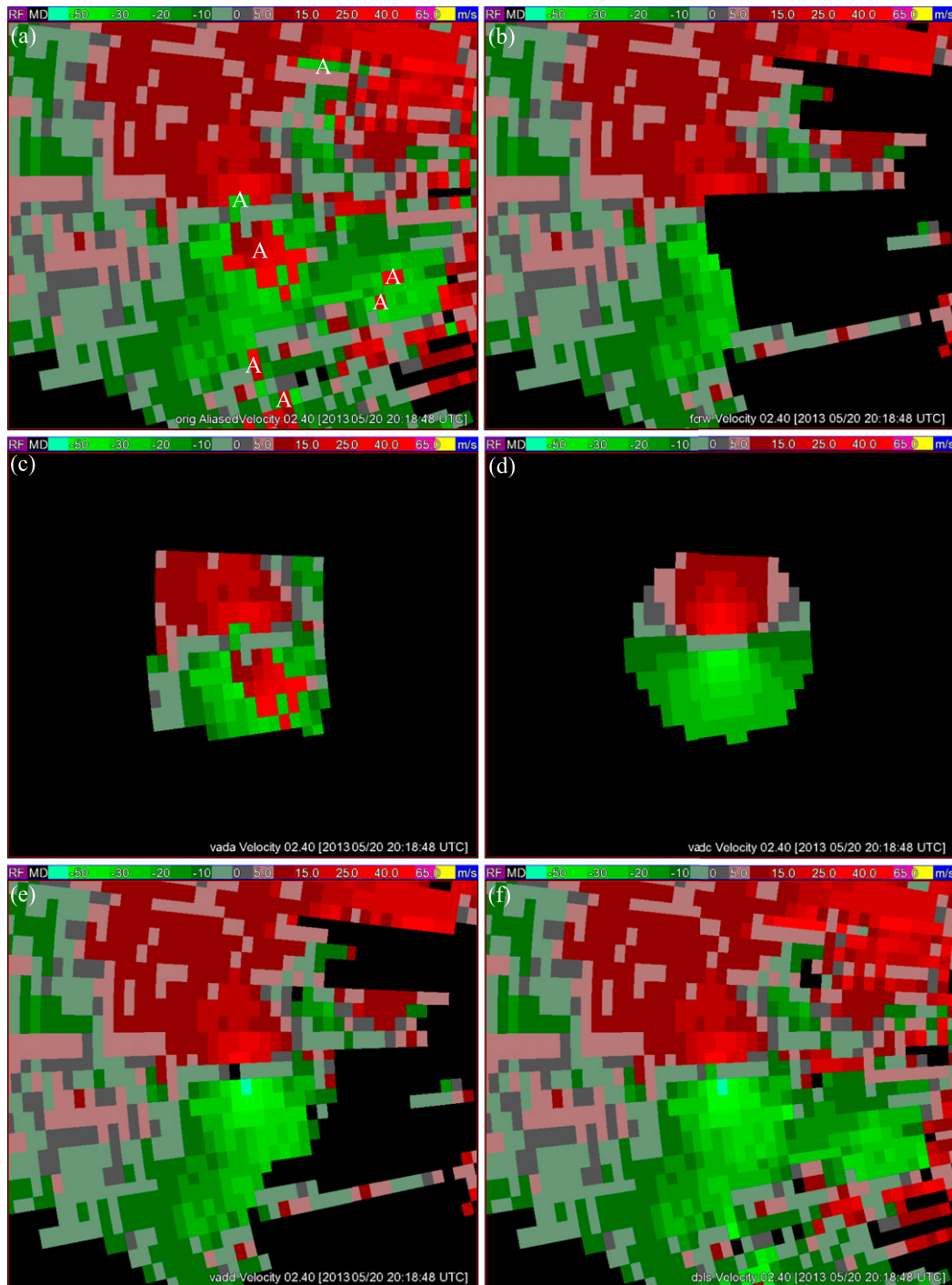$v_r > 0$ $(v_r < 0)$ for an outward (inward) radial-component velocity.

FIG. 3. As in Fig. 2, but for the mesocyclone detected from the KTLX radar scan on the 2.4° tilt (with $v_N = 26.12 \, \mathrm{m \, s^{-1}}$, $\Delta r = 0.25$ km, and $\Delta \phi = 1°$) at 2018:48 UTC 20 May 2013.

rare cases (from the 1182 volumes of data tested in this paper). The problem is minor for the other case (not shown) because it has only one erroneous velocity produced by the eAR-Var dealiasing.

b. Extensive tests with three datasets and summarized results

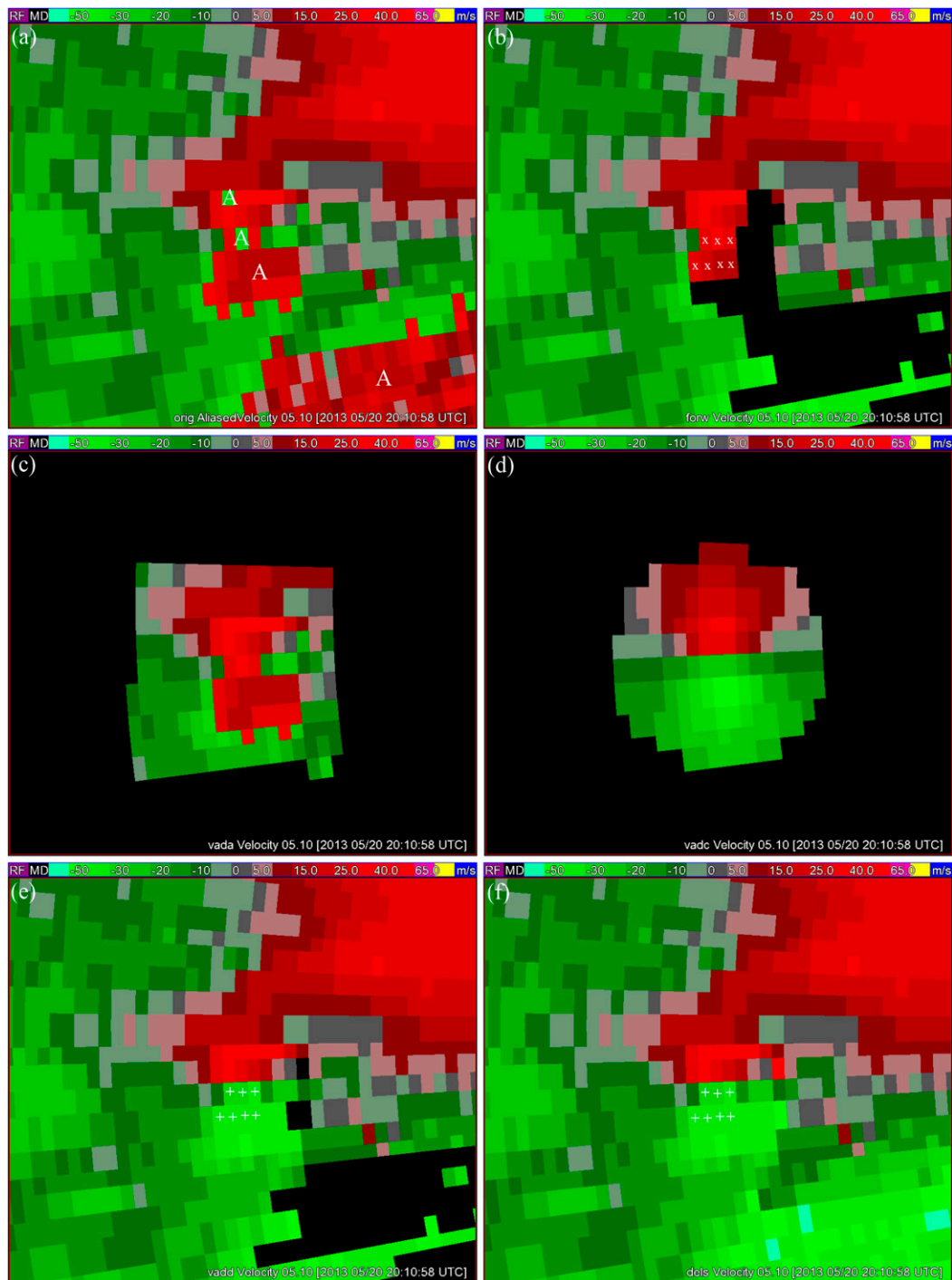The mesocyclone-targeted dealiasing is also tested extensively with three sets of severely aliased velocity

FIG. 4. As in Fig. 2, but for the mesocyclone detected from the KTLX radar scan on the 5.1° tilt (with $v_N =$ 26.12 m s^{-1}, $\Delta r = 0.25$ km, and $\Delta\phi = 1°$) at 2010:50 UTC 20 May 2013. The seven small white x's in (b) mark the seven erroneous velocities, respectively, and the seven small white + symbols in (e) and (f) mark the seven correctly dealiased velocities, respectively.

data collected by the operational KTLX, KVNX (Vance Air Force Base, Oklahoma), and KINX (Tulsa, Oklahoma) radars from tornadic storms that occurred in Oklahoma over three periods during the 2013 spring storm season. The first set, denoted by S1, contains 307 volumes of data collected from 2000 UTC 19 May to 0300 UTC 20 May. The second set, denoted by S2, contains 189 volumes of data collected from 1900 to

TABLE 1. Summary of results for the mesocyclone-targeted dealiasing tested with three sets of mesocyclone wind data, denoted by S1, S2 and S3, collected from the operational KTLX, KINX, and KVNX radars for three different periods (with S1 for 2000 UTC 19 May–0300 UTC 20 May, S2 for 1900 UTC–2300 UTC 20 May, and S3 for 1900 UTC 31 May–1200 UTC 1 Jun) during the 2013 spring storm season. For each dataset, the number of volumes tested is denoted by N_v and listed in column 2, the number of tilts with mesocyclones detected is denoted by N_t and listed in column 3, the number of tilts with not only mesocyclones detected but also data coverage conditions satisfied for performing the vortex wind analysis (see section 3a) is denoted by N_s and listed in column 4, and the number of vortex wind analyses performed and accepted (by the conditions in section 3b) is denoted by N_a and listed in column 5. The number of accepted but problematic analyses (that cannot be used safely without causing any error) is denoted by N_f and listed in column 6. In the last column, N_{Rej} is the number of rejected data by the eAR-Var dealiasing on the N_a tilts where the mesocyclone-targeted dealiasing is performed (with N_a accepted vortex wind analyses), and N_{Rec} is the number of recovered data by the mesocyclone-targeted dealiasing from the N_{Rej} rejected data. Hence, N_{Rec}/N_{Rej} is the recover rate (%).

Dataset	N_v	N_t	N_s	N_a	N_f	N_{Rec}/N_{Rej} (%)
S1	307	180	83	48	0	6.67
S2	189	88	57	48	0	11.29
S3	686	198	104	52	4	21.05
Total	1182	466	244	148	4	12.82

2300 UTC 20 May, and this set includes the 10 volumes tested in section 5a. The third set, denoted by S3, contains 686 volumes of data collected from 1900 UTC 31 May to 1200 UTC 1 June.

The test results with the abovementioned three datasets are summarized in Table 1. As shown in Table 1, from the 307 volumes of data in S1, mesocyclones are detected on 180 different tilts by the eAR-Var dealiasing. The data coverage conditions (see section 3a) are satisfied on 83 tilts among the abovementioned 180 tilts, so 83 vortex wind analyses are performed. Among the 83 analyses performed, 48 analyses can pass the acceptance conditions (see section 3b). All the 48 accepted analyses are used safely to recover rejected data with no error (as shown by $N_f = 0$ for S1 in column 6 of Table 1). Thus, for S1, the mesocyclone-targeted dealiasing can recover the rejected data very effectively and very cleanly (with no error) in and around the vortex core of the detected mesocyclone as long as the required data coverage conditions are satisfied for performing the AR vortex wind analysis and the acceptance conditions are satisfied for accepting the performed vortex wind analysis. The eAR-Var dealiasing is also free of error for S1, but it rejects many data in and around the vortex cores. On the 48 tilts where the mesocyclone-targeted dealiasing is performed (with the 48 accepted vortex wind analyses), the number of rejected data by the eAR-Var dealiasing

is $N_{Rej} = 823\,001$ and the number of raw data is $N_{Raw} = 5\,626\,796$, so the rejection rate is $N_{Rej}/N_{Raw} = 14.64\%$. From the N_{Rej} rejected data, the number of recovered data by the mesocyclone-targeted dealiasing is $N_{Rec} = 54\,867$, so the recover rate is $N_{Rec}/N_{Rej} = 6.67\%$ as listed for S1 in the last column of Table 1.

As shown further in Table 1, from the 189 volumes of data in S2, mesocyclones are detected on 88 tilts by the eAR-Var dealiasing. The data coverage conditions are satisfied on 57 different tilts among the 88 tilts. Among the 57 vortex wind analyses performed on the 57 tilts, 48 analyses can pass the acceptance conditions. All 48 accepted analyses are used safely to recover rejected data with no error (as shown by $N_f = 0$ for S2 in column 6 of Table 1). Thus, for S2, the mesocyclone-targeted dealiasing can recover the rejected data also very effectively and very cleanly in and around the vortex core of the detected mesocyclone as long as the required data coverage conditions and analysis acceptance conditions are satisfied. The effectiveness and related performances are exemplified in Figs. 2–4. The eAR-Var dealiasing is not completely free of error for S2, but it produces merely eight erroneous velocities in only two cases (including the worst case shown in Fig. 4b) among the extremely large number $(=2.01 \times 10^8)$ of raw data in S2. On the 48 tilts where the mesocyclone-targeted dealiasing is performed (with the 48 accepted vortex wind analyses), the number of rejected data by the eAR-Var dealiasing is $N_{Rej} = 355\,401$ and the number of raw data is $N_{Raw} = 5\,649\,766$, so the rejection rate is 14.64%. From the N_{Rej} rejected data, the number of recovered data by the mesocyclone-targeted dealiasing is $N_{Rec} = 40\,122$, so the recover rate is 11.29% as listed for S2 in the last column of Table 1.

Finally, as shown in Table 1, from the 686 volumes of data in S3, mesocyclones are detected on 198 tilts. The data coverage conditions are satisfied on 104 tilts among the 198 tilts. Among the vortex wind analyses performed on the 104 tilts, 52 analyses can pass the acceptance conditions. Among the 52 accepted analyses, 48 accepted analyses can be used safely to recover rejected data with no error, but the other 4 accepted analyses are problematic, as they cannot be used safely without causing any erroneous velocities (as shown by $N_f = 4$ for S3 in column 6 of Table 1). On the 52 tilts where the mesocyclone-targeted dealiasing is performed, the number of rejected data by the eAR-Var dealiasing is $N_{Rej} = 682\,584$ and the total number of raw data is $N_{Raw} = 9\,526\,874$, so the rejection rate is 7.16%. From the N_{Rej} rejected data, the number of recovered data by the mesocyclone-targeted dealiasing is $N_{Rec} = 143\,668$, so the recover rate is 21.05% as listed for S3 in the last column of Table 1.

In the abovementioned four problematic cases, spurious mesocyclones are falsely detected by the eAR-Var dealiasing. These four falsely detected mesocyclones are not filtered out by the data coverage conditions and analysis acceptance conditions. As explained in section 3, these two sets of conditions are imposed to ensure the reliability of the fitting and representativeness of the fitting results. Although these conditions may also filter out falsely detected mesocyclones in some cases, they are not designed for this in general and thus are not able to filter out falsely detected mesocyclones in the abovementioned four problematic cases. The detailed aspects of the problem are examined below for the case shown in Fig. 5.

As shown in Fig. 5a, only several raw velocities were aliased, so the coupled red (for $v_r^{ob} > 0$) and green (for $v_r^{ob} < 0$) image patterns in the central portion of the figure can still allow one to perceive qualitatively the presence of flow convergence and cyclonical shear along and around the zigzag boundary between the red and green image areas. The perceived cyclonic shear is neither well shaped nor strong enough to suggest the presence of mesocyclone, but a spurious mesocyclone is falsely detected by the eAR-Var dealiasing mainly due to the lack of adequate coverage of its dealiased seed data as shown by the long rejected data hole between the aforementioned two color image patterns in Fig. 5b.

Figure 5c shows the data-fitting area around the initially estimated vortex center (marked by the yellow • symbol). Since this data-fitting area is quite far (about 124 km) away from the radar site, its contained available data are sparse but satisfy the data coverage conditions. The AR vortex wind analysis is thus performed, and its produced reference velocities are shown in Fig. 5d together with its estimated vortex center location (marked by the yellow + symbol). This estimated vortex center location is not close to the initially estimated center (marked by the yellow • symbol), but it is still in the data-fitting area as shown in Fig. 5c. The estimated values of V_M ($=68.4\,\mathrm{m\,s^{-1}}$) and R_M ($=0.551\,\mathrm{km}$) are spurious, but they satisfy the acceptance conditions marginally. The reference velocities in Fig. 5d are thus mostly incorrect, so the reference check recovers only two rejected data but produces five erroneous velocities as marked by the small white x symbols in Fig. 5e. After this, the continuity check produces two more erroneous velocities as shown in Fig. 5f, although it correctly recovers 6720 rejected data (not fully shown) over the entire tilt. In this case, unlike the case in Fig. 4, the reference check cannot be extended safely to recheck dealiased seed data produced by the eAR-Var dealiasing, and the extension will produce 12 more erroneous velocities (not shown) for the problematic case in Fig. 5.

In three other problematic cases (not shown), erroneous velocities are also produced in small numbers (<10 in each case) and the problems are again primarily caused by falsely detected mesocyclones from the eAR-Var dealiasing. Thus, from our extensive tests with the three sets (a total of 1182 volumes), the mesocyclone-targeted dealiasing is found to be effective in recovering the rejected velocity data with almost no error (at least no serious error) in and around the vortex core of the detected mesocyclone, provided the required data coverage conditions and the analysis acceptance conditions are satisfied. As summarized for all three datasets in the last row of Table 1, the mesocyclone-targeted dealiasing is performed on 148 tilts (with 148 accepted vortex wind analyses). On these 148 tilts, the number of rejected data by the eAR-Var dealiasing is $N_{\mathrm{Rej}} = 1\,860\,986$ and the number of recovered data by the mesocyclone-targeted dealiasing is $N_{\mathrm{Rec}} = 238\,657$, so the averaged recover rate is $N_{\mathrm{Rec}}/N_{\mathrm{Rej}} = 12.82\%$ for the three datasets as listed in the last column of Table 1. Note that the rejected data are mostly well recovered in the vortex core and vicinity areas as shown by the examples in Figs. 2–4, so the local recover rates in these critical areas can be much higher than the averaged rate of 12.82% over the entire 148 tilts.

6. Conclusions

A mesocyclone-targeted dealiasing routine is developed in this paper to perform two additional steps after the eAR-Var dealiasing (developed and named as model+AR-Var-based dealiasing in X13)—that is, a reference check performed first to recover the rejected data in the vortex core followed by a continuity check to recover the remaining rejected data around and beyond the vortex core of the mesocyclone detected by the eAR-Var dealiasing. For the reference check performed in the first step, the required reference velocity is produced by an AR vortex wind analysis designed specifically for mesocyclones. This AR vortex analysis uses the same vortex model as that used in X14 for tropical cyclones, but it retains all six control parameters in the modeled velocity [see (3) and (4)] and its constructed cost function [see (5)]. As these six parameters can be reasonably well estimated at the global minimum of the cost function in cases where the mesocyclone is correctly detected and the required data coverage conditions and analysis acceptance conditions (described in section 3) are satisfied, they not only produce the required reference velocity for the dealiasing developed in this paper but also provide an accurately estimated vortex center location to improve the vortex wind analysis for nowcast applications (Xu et al. 2015).
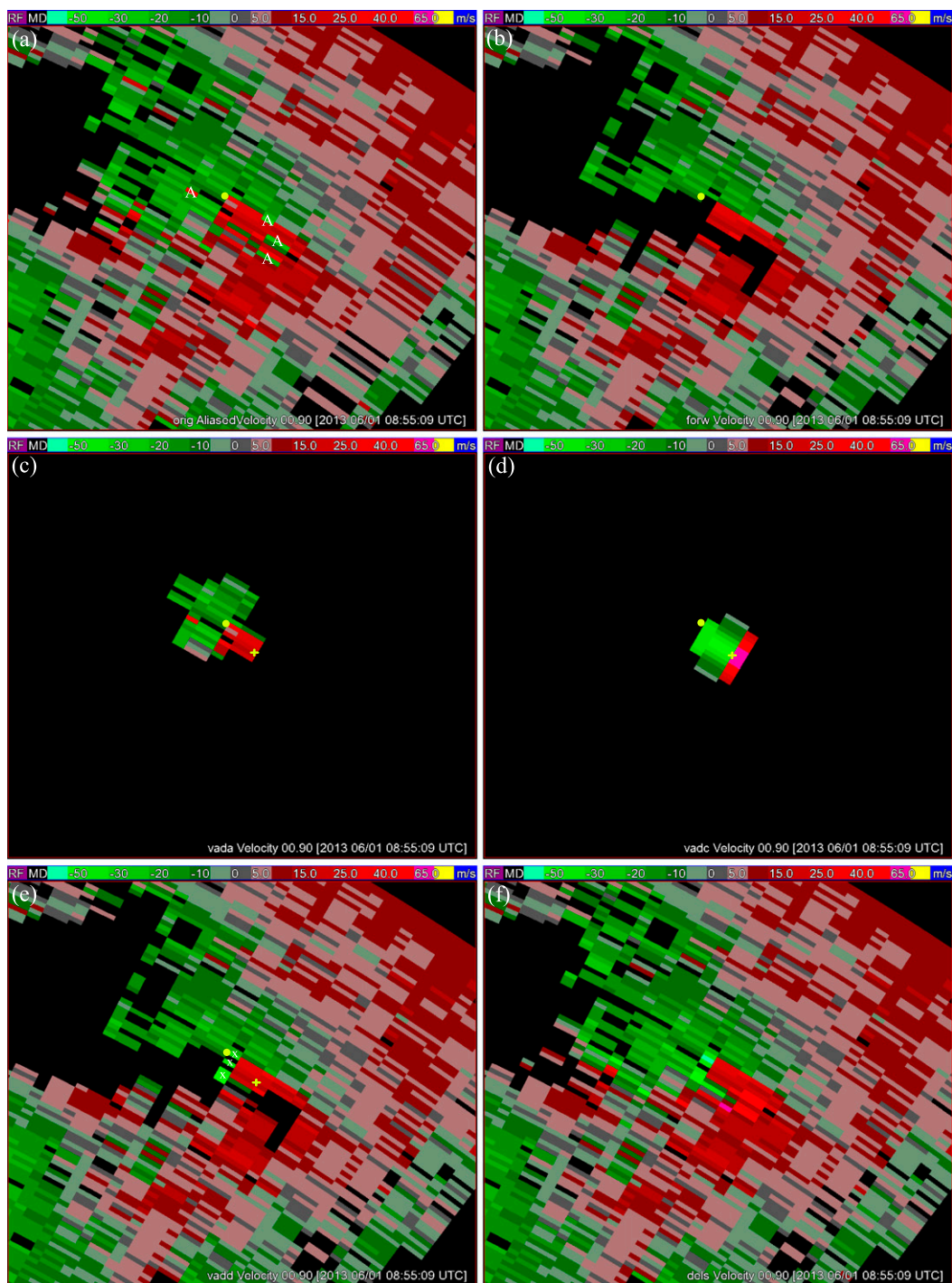
FIG. 5. As in Fig. 2, but for the mesocyclone detected from the KTLX radar scan on the 0.9° tilt (with v_N = 28.22 m s^{-1}, Δr = 0.25 km, and $\Delta\phi$ = 0.5°) at 0855:09 UTC 1 Jun 2013. The yellow • symbol in (a)–(e) marks the initially estimated vortex center of the falsely detected mesocyclone by the eAR-Var dealiasing. The yellow + symbol in (c)–(e) marks the final falsely estimated vortex center by the AR vortex wind analysis. The three small white x's in (e) mark the areas covered by five erroneous velocities.

Since the AR vortex wind analysis designed for mesocyclones needs only to fit a limited number of data in the data-fitting area (see Figs. 2b, 3b, or 4b), the mesocyclone-targeted dealiasing is computationally efficient for real-time application. Typically, with its two steps performed after the eAR-Var dealiasing, the CPU time for processing the entire volume of aliased velocity data scanned from tornadic storms is increased from about 90 s (used by the eAR-Var dealiasing) to only about 120 s in total on a Dell XII computer.

Tested extensively with severely aliased velocity data collected by operational WSR-88D radars from tornadic storms (see the summary in Table 1), the mesocyclone-targeted dealiasing is found to be effective and efficient in recovering the rejected data with almost no error (at least no serious error) in and around the vortex core of the detected mesocyclone for which the required data coverage conditions and analysis acceptance conditions are satisfied. Small numbers (<10 in each case) of erroneous velocities are found in only four cases, and they are primarily caused by falsely detected mesocyclones from the eAR-Var dealiasing. These four falsely detected mesocyclones are not filtered out by the data coverage conditions and analysis acceptance conditions, because these conditions are designed for ensuring the reliability and realism of the AR vortex wind analysis (although they can also filter out falsely detected mesocyclones in some cases). Further investigation and improvement beyond this study are required to further reduce false detections.

The eAR-Var dealiasing is also almost—but not absolutely—free of errors for the data (1182 volumes) tested in this paper, and erroneous velocities are produced merely in two extremely rare cases. One case has seven erroneous velocities in the vortex core area (as shown in Fig. 4b), and the other case has only one erroneous velocity also in the vortex core (not shown). These erroneous velocities can be detected and corrected by the reference check in the first step of the mesocyclone-targeted dealiasing if the reference check is extended to not only recover rejected data but also correct erroneous velocities among the accepted seed data produced by the eAR-Var dealiasing in the vortex core. This extension, however, cannot be used safely (with no error) if a mesocyclone is falsely detected by the eAR-Var dealiasing.

Note that the extended AR-Var analysis in X13 and the AR vortex wind analysis in X14 and Jiang and Xu (2016) are all one-dimensional, as they use only one-dimensional data along a single range circle selected from each tilt within a given vertical layer. In contrast, the AR vortex wind analysis designed for mesocyclones in this paper is two-dimensional, as it uses two-dimensional data over the mesocyclone vortex core area on each tilt

of radar scan where a mesocyclone is detected. It is possible to extend the one-dimensional AR-Var analysis into a two-dimensional analysis over a sector area to cover a cluster of isolated data far away from the radar and thus improve the dealiased data coverage in isolated data areas. Such a two-dimensional extension is under investigation.

REFERENCES

Burgess, D. W., and T. D. Crum, 2009: Observed failure modes of the WSR-88D velocity dealiasing algorithm during severe weather outbreaks. *34rd Conf. on Radar Meteorology*, Williamsburg, VA, Amer. Meteor. Soc., P5.16. [Available online at https://ams.confex.com/ams/34Radar/techprogram/paper_156056.htm.]

Eilts, M. D., and S. D. Smith, 1990: Efficient dealiasing of Doppler velocities using local environment constraints. *J. Atmos. Oceanic Technol.*, **7**, 118–128, doi:10.1175/1520-0426(1990)007<0118:EDODVU>2.0.CO;2.

Gao, J., K. K. Droegemeier, J. Gong, and Q. Xu, 2004: A method for retrieving mean horizontal wind profiles from single-Doppler radar observations contaminated by aliasing. *Mon. Wea. Rev.*, **132**, 1399–1409, doi:10.1175/1520-0493-132.1.1399.

Gong, J., L. Wang, and Q. Xu, 2003: A three-step dealiasing method for Doppler velocity data quality control. *J. Atmos. Oceanic Technol.*, **20**, 1738–1748, doi:10.1175/1520-0426(2003)020<1738:ATDMFD>2.0.CO;2.

Jiang, Y., and Q. Xu, 2016: An adaptive dealiasing method for Doppler velocities scanned from hurricanes and typhoons. *J. Atmos. Oceanic Technol.*, **33**, 1931–1947, doi:10.1175/JTECH-D-15-0146.1.

Jing, Z., and G. Wiener, 1993: Two-dimensional dealiasing of Doppler velocities. *J. Atmos. Oceanic Technol.*, **10**, 798–808, doi:10.1175/1520-0426(1993)010<0798:TDDODV>2.0.CO;2.

Liu, S., and Coauthors, 2009: WSR-88D radar data processing at NCEP. *34rd Conf. on Radar Meteorology*, Williamsburg, VA, Amer. Meteor. Soc., 14.2. [Available online at https://ams.confex.com/ams/34Radar/techprogram/paper_156011.htm.]

Smith, T. M., and K. L. Elmore, 2004: The use of radial velocity derivatives to diagnose rotation and divergence. *11th Conf. on Aviation, Range and Aerospace*, Hyannis, MA, Amer. Meteor. Soc., P5.6. [Available online at https://ams.confex.com/ams/11aram22sls/techprogram/paper_81827.htm.]

Stumpf, G. J., A. Witt, E. D. Mitchell, P. L. Spencer, J. T. Johnson, M. D. Eilts, K. W. Thomas, and D. W. Burgess, 1998: The National Severe Storms Laboratory mesocyclone detection algorithm for the WSR-88D. *Wea. Forecasting*, **13**, 304–326, doi:10.1175/1520-0434(1998)013<0304:TNSSLM>2.0.CO;2.

Vatistas, G. H., V. Kozel, and W. C. Mih, 1991: A simpler model for concentrated vortices. *Exp. Fluids*, **11**, 73–76, doi:10.1007/BF00198434.

Witt, A., R. A. Brown, and Z. Jing, 2009: Performance of a new velocity dealiasing algorithm for the WSR-88D. *34rd Conf. on Radar Meteorology*, Williamsburg, VA, Amer. Meteor. Soc., P4.8. [Available online at https://ams.confex.com/ams/34Radar/techprogram/paper_155951.htm.]

Xu, Q., 2009: Bayesian perspective of the unconventional approach for assimilating aliased radar radial velocities. *Tellus*, **61A**, 631–634, doi:10.1111/j.1600-0870.2009.00413.x.

——, and K. Nai, 2012: An adaptive dealiasing method based on variational analysis for radar radial velocities scanned with small Nyquist velocities. *J. Atmos. Oceanic Technol.*, **29**, 1723–1729, doi:10.1175/JTECH-D-12-00145.1.

——, and ——, 2013: A two-step variational method for analyzing severely aliased radar velocity observations with small Nyquist velocities. *Quart. J. Roy. Meteor. Soc.*, **139**, 1904–1911, doi:10.1002/qj.2075.

——, ——, L. Wei, and Q. Zhao, 2009: An unconventional approach for assimilating aliased radar radial velocities. *Tellus*, **61A**, 621–630, doi:10.1111/j.1600-0870.2009.00412.x.

——, ——, and ——, 2010: Fitting VAD winds to aliased Doppler radial-velocity observations: A global minimization problem in the presence of multiple local minima. *Quart. J. Roy. Meteor. Soc.*, **136**, 451–461, doi:10.1002/qj.589.

——, ——, ——, P. Zhang, S. Liu, and D. Parrish, 2011: A VAD-based dealiasing method for radar velocity data quality control. *J. Atmos. Oceanic Technol.*, **28**, 50–62, doi:10.1175/2010JTECHA1444.1.

——, ——, S. Liu, C. Karstens, T. Smith, and Q. Zhao, 2013: Improved Doppler velocity dealiasing for radar data assimilation and storm-scale vortex detection. *Adv. Meteor.*, 2013, 562386, doi:10.1155/2013/562386.

——, Y. Jiang, and L. Liu, 2014: Fitting parametric vortices to aliased Doppler velocities scanned from hurricanes. *Mon. Wea. Rev.*, **142**, 94–106, doi:10.1175/MWR-D-12-00362.1.

——, L. Wei, and K. Nai, 2015: Analyzing vortex winds in radar-observed tornadic mesocyclones for nowcast applications. *Wea. Forecasting*, **30**, 1140–1157, doi:10.1175/WAF-D-15-0046.1.

Zhang, J., and S. Wang, 2006: An automated 2D multipass Doppler radar velocity dealiasing scheme. *J. Atmos. Oceanic Technol.*, **23**, 1239–1248, doi:10.1175/JTECH1910.1.